Effect of Artificial Saliva Modification on Corrosion Resistance and Electronic Properties of Bego Wirobond C Dental Alloy

Bożena Łosiewicz *, Patrycja Osak, Julian Kubisztal, Karolina Górka-Kulikowska

Posted Date: 19 October 2023

doi: 10.20944/preprints202310.1223.v1

Keywords: electrochemical impedance spectroscopy; CoCrMo dental alloy; pitting corrosion; artificial saliva

Article

Effect of Artificial Saliva Modification on Corrosion Resistance and Electronic Properties of Bego Wirobond® C Dental Alloy

Bożena Łosiewicz [1,*], Patrycja Osak [1], Julian Kubisztal [1] and Karolina Górka-Kulikowska [2]

[1] University of Silesia in Katowice, Faculty of Science and Technology, Institute of Materials Engineering, 41-500 Chorzów, Poland; patrycja.osak@us.edu.pl (P.O.); julian.kubisztal@us.edu.pl (J.K.)

[2] Poznan University of Medical Sciences, Department of Biomaterials and Experimental Dentistry, 60-812 Poznań, Poland; karolinagorka.profil@gmail.com (K.G.)

* Correspondence: bozena.losiewicz@us.edu.pl; Tel.: +48-32-3497-527

Abstract: Wirobond® C is a commercial dental casting alloy suitable for the fabrication of crowns, bridges as well as metal-ceramic restorations. This work aims with the study of the effect of ready-to-use Listerine® and Meridol® mouthwashes and sodium fluoride on corrosion resistance of the CoCrMo dental alloy to electrochemical corrosion in artificial saliva at 37 °C. SEM, EDS, SKP, and microhardness investigations were carried out to characterize the material under study. In vitro corrosion resistance of the CoCrMo alloy was conducted by the open circuit potential method, electrochemical impedance spectroscopy, and anodic polarization curves. The presence of Co 59.8(8) wt.%, Cr 31.5(4) wt.%, and Mo 8.8(6) wt.% was confirmed. The CoCrMo alloy was characterized by Vickers microhardness of 445(31) $\mu HV_{0.3}$. Based on EIS data, the capacitive behavior and high corrosion resistance of CoCrMo alloy was revealed. The kinetics of pitting corrosion in the artificial saliva was lower after the modification with NaF and Listerine® and Meridol® mouthwashes. The potentiodynamic characteristics revealed the passive behavior of CoCrMo alloy in all solutions. Based on the SKP measurements of the CoCrMo alloy after corrosion tests, the effect of artificial saliva modification on electronic properties of Bego Wirobond® C dental alloy was found.

Keywords: electrochemical impedance spectroscopy; CoCrMo dental alloy; pitting corrosion; artificial saliva

1. Introduction

The requirements that a dental metal biomaterial must meet for applications with living tissue are primarily biocompatibility in the tissues and fluids of the dental organ as well as good corrosion resistance, tissue compatibility, resistance to abrasive wear, appropriate electrical properties, lack of initiation of unfavorable reactions in peri-implant tissues, specific mechanical properties, and acceptable manufacturing costs. Corrosion of dental alloys may have biological, functional, and aesthetic consequences. The biological consequences are of the greatest importance. Metallic construction biomaterials introduced into the oral cavity contribute to the formation of electrochemical phenomena. These phenomena have a negative impact both locally and generally on the human body. Therefore, metallic materials' corrosion resistance is a very important factor influencing their suitability in prosthetic applications [1–8].

Metal materials constitute the widest group of biomaterials used in dental prosthetics, oral surgery, and orthodontics. Precious and base metals and their alloys are mainly used in dental prosthetics. Precious metals such as gold and platinum have been used for many years, but for economic reasons, their use has been significantly limited [10,11]. Titanium [1–3,5,6,8,12,13] and cobalt [14–17] alloys are widely used in dental prosthetics, which is why they have taken a permanent position in dental practice instead of precious metals. Metal materials used for the production of implants can be divided into short-term ones, the duration of which should not exceed two years in the human body, including cobalt alloys and austenitic steels and long-term ones, such as titanium

 doi:10.20944/preprints202310.1223.v1

and its alloys, where the service life can reach up to 25 years. The currently used cobalt alloys can be divided into three groups: (*i*) Vitalium-type foundry alloys, (*ii*) wrought alloys, and (*iii*) alloys produced by powder metallurgy. Cobalt-casting alloys are the most frequently used materials for the production of components used for biomedical implants [14–17]. Cobalt-based alloys are classified as materials with good biotolerance, resulting from the presence of a passive layer on their surface. This layer is mainly composed of chromium oxide, which is formed spontaneously. Their suitability for implantation was determined by their greater biocompatibility in the environment of tissues and body fluids than the austenitic CrNiMo steels and Ti6Al4V alloy, as well as their greater resistance to pitting and crevice corrosion and their lower susceptibility to initiating fatigue cracks. The tendency of the CoCrMo alloy to crevice corrosion is ten times lower than that of CrNiMo steel. These alloys also show good resistance to pitting and crevice corrosion in chloride solutions and physiological salts. Their mechanical properties and corrosion resistance are determined by their chemical composition and structure, which depends on the type of technology and manufacturing conditions. In this respect, they can be divided into foundry and plastically processed. Mainly prosthetic implants are made from casting alloys. However, plastically processed alloys are sometimes used to produce plates, bone screws, points, wires, and shaped elements for anastomoses, as well as frames of removable dentures [15–17].

When testing the corrosion resistance of dental alloys in vitro, the aim is to obtain conditions most similar to those in the oral cavity [1,2,13–15]. Due to the very low corrosion rate of dental alloys, corrosion symptoms are not visually noticeable in most cases. This limits in vivo corrosion testing, which can only be performed in cases where the corroding metal components are removable. An increase in interest in the CoCrMo alloy has been observed in the literature in recent years [14–17]. This alloy is widely used in dental practice. An increasing number of publications are devoted to electrochemical tests using electrochemical impedance spectroscopy (EIS), which provides more research possibilities compared to direct current methods and allows us to determine in detail the mechanism and kinetics of electrochemical corrosion.

The main aim of this work is therefore to determine the corrosion resistance of the CoCrMo dental alloy in a standard corrosive environment of 0.9% NaCl solution (saline) by the ISO 10271 standard [18] and in solutions of modified artificial saliva. Artificial saliva solutions with neutral and acidic pH were modified with NaF, which is the main ingredient of toothpastes and mouthwashes with alcoholic (Meridol®) and aqueous (Listerine®) solvents. Classic electrochemical methods, such as the open circuit potential method and the anodic polarization curve method, were used to determine in detail the mechanism and kinetics of electrochemical corrosion, combined with the complementary EIS research technique. The effect of modification of the corrosion environment on the electronic properties of the CoCrMo alloy is also discussed.

2. Materials and Methods

2.1. Surface Preparation of Samples

The biomaterial under study was a dental Wirobond® C cobalt-chrome metal-to-ceramic alloy (BEGO Bremer Goldschlägerei Wilh. Herbst GmbH & Co. KG, Bremen, Germany), which complies with ISO 22674 [19] and ISO 9693-1 [20]. The Wirobond® C is produced in accordance with ISO 13485 [21] and is approved as a class IIa medical device. This alloy is commercially used for the fabrication of prosthetic restorations or sections thereof with thin cross-sections exposed to very high loads, e.g. removable partial dentures, clasps, veneered crowns, long-span bridgework or bridges with small cross-sections, bars, retainers, implant-supported superstructures (Figure 1).

Preprints (www.preprints.org) | NOT PEER-REVIEWED | Posted: 19 October 2023 doi:10.20944/preprints202310.1223.v1

(**a**) (**b**) (**c**)

Figure 1. Wirobond® C dental alloy: (**a**) [22]; (**b**) In the dental and prosthetic office used for partial dentures [23]; (**c**) In trading condition available as cylinders [24].

The Wirobond® alloy does not contain nickel, cadmium, beryllium, and lead. It is intended primarily for patients allergic to nickel. Cerium in its chemical composition ensures high bond strength with the ceramic, minimising the risk of subsequent flaking or chipping. This cobalt-based dental casting alloy does not cause a chemical reaction in the patient's mouth. It does not require oxidation. It is characterized by simple processing and casting, carbon-free composition especially suitable for laser welding, high adhesion to ceramics, low heat conductivity ensuring pulp protection and high wearing comfort for the patient (Table 1). The Wirobond® alloy is biocompatible, corrosion resistant thanks to a firmly-adhering passive layer and can be easily laser welded. It is as flexible as precious metals. No cytotoxic potential was determined in accordance with the ISO 10993-5 standard [25].

Table 1. Wirobond® C dental alloy characteristics.

Parameter	Value
Type (accord. to ISO 22674)	4
Density	8.5 g cm ^{3}
Preheating temperature	900 1,000 °C
Solidus, liquidus temperature	1,360 °C, 1,420 °C
Casting temperature	1,500 °C
Young's modulus	180 GPa
Proof strength ($R_{p0.2}$)	440 MPa
Ultimate strength (Rm)	780 MPa
Elongation after fracture	16 %
Vickers hardness	310 HV10
Coefficient of thermal expansion (CTE) 25 500 °C, 10 ^{6} K ^{1}	14.3

The Wirobond® C dental alloy was provided in the form of cylinders from which disc-shaped samples were cut with 3 mm in thickness. The samples were included in graphite using an ATM Opal 400 hot mounting press (Spectrographic Ltd., Guiseley, Leeds, UK) at a pressure of 3.5 bars at 180 °C for 10 minutes. The included samples were ground using the metallographic grinding and polishing machine Metkon Forcipol 102 (Metkon Instruments Inc., Bursa, Turkey) on P320-P2500 abrasive papers (Buehler Ltd., Lake Bluff, IL, USA) and polished using a colloidal SiO_2 suspension (0.04 µm grain size, Struers, Cleveland, OH, USA). The polished samples were degreased in acetone (Avantor Performance Materials Poland S.A., Gliwice, Poland) for 20 minutes using an ultrasonic cleaner USC-TH (VWR International, PA, USA), and then sonicated in ultrapure water (Milli-Q Advantage A10 Water Purification System, Millipore SAS, Molsheim, France) for 20 minutes.

2.2. SEM and EDS Study of the CoCrMo Alloy

Microstructure investigations of CoCrMo alloy were conducted using a JEOL JSM-6480 scanning electron microscope (SEM, Peabody, MA, USA). A resolution of 3 nm and a

 doi:10.20944/preprints202310.1223.v1

voltage acceleration of 20 kV were applied. The microanalysis of local chemical composition of the samples was performed using the EDS method.

2.3. Microhardness of the CoCrMo Alloy

Micromechanical properties of the CoCrMo alloy were examined in the microhardness test using a Wilson®–WolpertTM Microindentation Tester 401MVD (Wilson Instruments, LLC, Carthage, TX, USA). The Vickers method was used in the study with a Vickers indenter as a square-based pyramidal-shaped diamond indenter with face angles of 136 ° by the ISO 6507-1:2018 standard [26]. A hardness scale was HV = 0.1. A maximum indentation load of 0.3 N was used for 10 to 15 seconds.

2.4. Corrosion Resistance of the CoCrMo Alloy

The in vitro corrosion resistance of the CoCrMo electrode to electrochemical corrosion was conducted in artificial saliva solution of pH 7.4(1) and pH 5.5(1) by the AFNOR/NF standard S90-701 [27]. The artificial saliva solutions modifiers were 0.1 M NaF solution and 15 mL of commercial antiseptic mouthwash Listerine Total Care Teeth Protection® (McNeil Consumer Healthcare McNeil-PPC, Inc., Fort Washington, PA, USA) based on alcohol (21.6 % v/v), and Meridol® (Colgate-Palmolive Company, NY, USA) alcohol-free. For comparison, a 3.5% NaCl solution (saline) of pH 7.4(1) by the ISO 10271:2021 standard was also used [18]. All solutions were prepared using ultrapure water and reagents pure for chemical analysis (Avantor Performance Materials Poland S.A., Gliwice, Poland).

An electrochemical cell with a three-electrode configuration was used, in which the working electrode (WE) was the CoCrMo alloy, the counter electrode (CE) was a Pt foil, and the reference electrode (RE) was a saturated calomel electrode (SCE). Electrochemical measurements were conducted at 37(2) °C in deaerated solutions by the ISO 10271:2021 standard [18] using the Autolab/PGSTAT12 (Metrohm Autolab B.V., Utrecht, The Netherlands). Open circuit potential (E_{OC}) was registered for a time (t) of 2 h. EIS spectra were recorded at the E_{OC} in the range of frequency (f) 20 kHz-10 mHz. An amplitude of the sinusoidal signal was 10 mV. Electrical equivalent circuits using the EQUIVCRT program with the circuit description code by Boukamp [28] and the complex non-linear least squares (CNLS) method were used to interpret the EIS spectra. Anodic polarization curves were recorded in the potential range from 150 mV more negative than E_{OC} to 1 V at a polarization rate of 1 mVs^{-1}.

2.5. Scanning Kelvin Probe Measurements of the CoCrMo Alloy

The electronic properties of the CoCrMo alloy before and after corrosion tests were studied by non-contact scanning Kelvin probe (SKP) method in the air. The M370 scanning electrochemical workstation (Prinston Applied Research) with the built-in SKP370 module and the VCAM3 optical video microscope was applied with the tungsten microprobe U-SKP-150 (Uniscan Instruments) of 150 µm diameter. The microprobe tip was approximately 100 µm away from the sample surface. The scanning was performed for an area of 2.5 x 2 mm^2. Changes in the contact potential difference (CPD) distribution on the surface of samples were determined using the height tracking mode. The microprobe scanned at a sweep scan mode with a velocity of 20 µm s^{-1}. The Scanning Electrochemical Work Station M370 Version 2.45 software was used for measurements and analysis of the results obtained.

3. Results and Discussion

3.1. Microstructure and Chemical Composition of the CoCrMo Alloy

To control the chemical composition of the CoCrMo alloy, the inlcuded samples as shown in Figure 2a were studied using the EDS method. Figure 2b presents the SEM image of the surface morphology of the tested alloy in the microregion selected for EDS microanalysis. The exemplary EDS spectrum is displayed in Figure 2c. Based on the binding energy of characteristic peaks, the

Preprints (www.preprints.org) | NOT PEER-REVIEWED | Posted: 19 October 2023 doi:10.20944/preprints202310.1223.v1

presence of Co 59.8(8) wt.%, Cr 31.5(4) wt.%, and Mo 8.8(6) wt.%. The obtained chemical composition results are in very good agreement with the chemical composition provided by the manufacturer of the CoCrMo alloy.

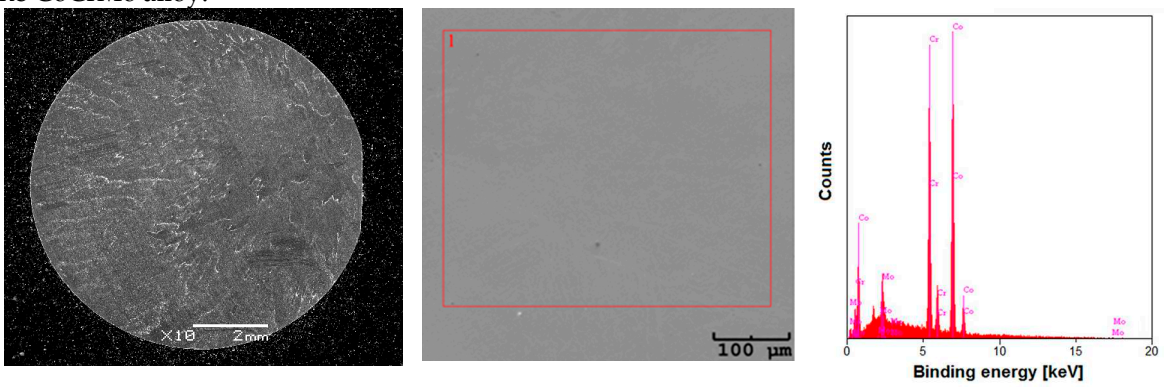

(**a**) (**b**) (**c**)

Figure 2. The commercial CoCrMo alloy: (**a**) SEM image of the sample after inclusion in graphite; (**b**) SEM image of the surface morphology in the selected microregion selected for EDS microanalysis; (**c**) EDS spectrum collected in the investigated microregion.

3.2. Micromechanical Properties of the CoCrMo Alloy

The Vickers microhardness tests were performed for two samples of the CoCrMo alloy at 10 measuring points. The obtained results of the Vickers microhardness are presented in Table 2.

Table 2. Results of the Vickers microhardness for the Wirobond® C dental alloy.

Number of measurement	Sample 1 [µHV$_{0.3}$]	Sample 2 [µHV$_{0.3}$]
1	432	468
2	415	418
3	505	414
4	475	456
5	450	488
6	404	472
7	410	453
8	440	401
9	467	417
10	480	443
Average value	445	
Standard deviation	31	

The Vickers microhardness test was performed on samples in the initial state. Based on the obtained results, it is shown that the samples that were tested are characterized by similar microhardness values and the average Vickers microhardness is 445(31) µHV$_{0.3}$. The alloy owes its high microhardness to the presence of Cr, which increases the resistance to shape change [29].

3.3. In Vitro Electrochemical Tests Using the Open Circuit Potential Method

A summary of the experimentally obtained relationships $E_{OC} = f(t)$ for the CoCrMo electrode in artificial saliva solution before and after modification and comparatively in physiological saline is presented in Figure 3. From the course of the obtained $E_{OC} = f(t)$ curves for the tested electrode in the corrosion environments used, it is possible to conclude about the ability of the CoCrMo alloy to self-

Preprints (www.preprints.org) | NOT PEER-REVIEWED | Posted: 19 October 2023 doi:10.20944/preprints202310.1223.v1

passivation in the environment of body fluids and physiological saline and to initially predict the rate of corrosion changes occurring on the surface of the tested material.

After approximately 7200 seconds, the ion-electron equilibrium was established at the interface between the surface of the tested electrode and all the electrolytes used, resulting in a stabilized E_{OC} value. The most negative E_{OC} value of –317(63) mV was recorded for the CoCrMo alloy in artificial saliva solution with pH = 7.4 [30], which indicates the lowest corrosion resistance of the tested alloy. In an artificial saliva solution with pH = 5.5, which simulates the inflammation of the body, the E_{OC} value increases more than threefold, and in a physiological saline solution with pH = 7.4, it increases more than one and a half times compared to an artificial saliva solution with physiological pH. The obtained $E_{OC} = f(t)$ characteristics also indicate that modification of the artificial saliva solution with both pH = 7.4 and pH = 5.5 causes an increase in the E_{OC} value for the CoCrMo electrode. The tested electrode showed the highest open circuit potential value in artificial saliva solution with pH = 5.5 with the addition of 0.1 M NaF, E_{OC} = –53(10) mV.

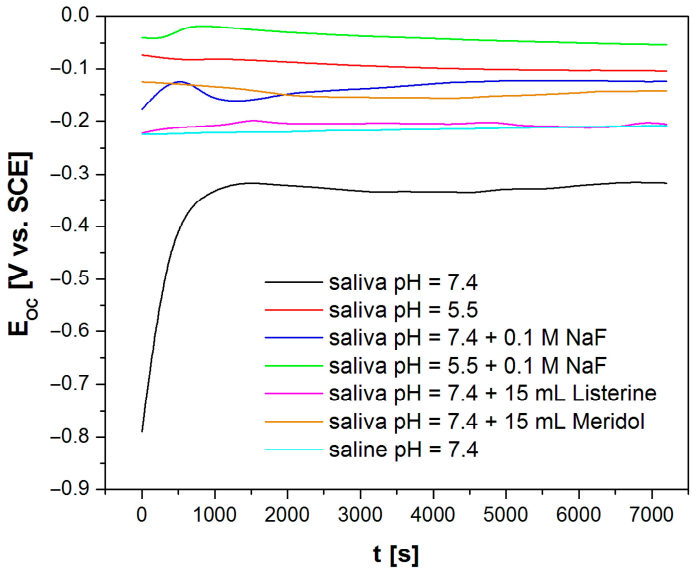

Figure 3. The relationship $E_{OC} = f(t)$ for the CoCrMo electrode in the applied corrosion environments at 37 °C.

After modification of artificial saliva solution with pH = 7.4 with Listerine® and Meridol® mouthwashes, the E_{OC} value for the CoCrMo electrode increases to –0.205(41) mV and –0.143(28) mV, respectively. Further electrochemical measurements were carried out assuming that the obtained E_{OC} values could be treated as approximate corrosion potential (E_{cor}).

3.4. In Vitro Electrochemical Study Using Electrochemical Impedance Spectroscopy

To determine the mechanism and kinetics of electrochemical corrosion occurring on the surface of the CoCrMo electrode in the environment of artificial saliva before and after modification, and comparatively in a saline, a complementary method of electrochemical impedance spectroscopy (EIS) was used.

Figure 4 shows the CPE1 model used, consisting of the electrolyte resistance (R_s) and a parallel system of a constant-phase element (CPE) combined with the charge transfer resistance (R_{ct}). The best fitting of the experimental EIS data with the software-generated model curve for the real and imaginary part of the circuit impedance was obtained depending on the frequency of changes in the measurement signal for all corrosive environments used (Figures 5–7). The CPE1 equivalent electrical circuit with a one-time constant is characteristic of an electrode material with an undifferentiated surface morphology, with shallow pits on the surface. For the purposes of CNLS fitting, CPE was used instead of a capacitor, which was treated in the considerations as a "leaky" capacitor with a non-zero real and imaginary components. The CPE impedance ($\hat{Z}_{CPE}$) is given by Equation (1) [31]:

Preprints (www.preprints.org) | NOT PEER-REVIEWED | Posted: 19 October 2023 doi:10.20944/preprints202310.1223.v1

$$\hat{Z}_{CPE} = \frac{1}{T(j\omega)^{\phi}}. \quad (1)$$

where T [F cm $^{-2}$ s$^{\phi-1}$] is a capacitive parameter which is a function of the electrode potential, and the dimensionless parameter ϕ is the angle of rotation of the purely capacitive line on the Nyquist plot, $\alpha = 90°(1 - \phi)$.

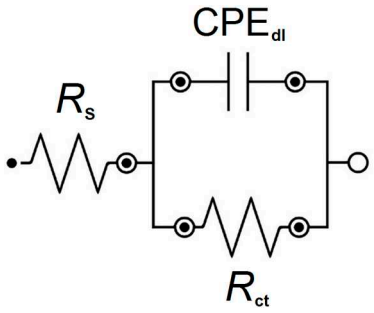

Figure 4. CPE1 model of equivalent electrical circuit for the pitting corrosion of CoCrMo electrode in the biological environment.

In the Nyquist spectral spectrum for the CoCrMo electrode in all tested corrosion environments, only one semicircle is observed in the entire range of tested frequencies, the radius of which depends on the type of corrosion environment (Figure 5). As a result of adding modifiers in the form of NaF and mouthwashes to the artificial saliva environment, there is a tendency for the recorded semicircle in the spectrum to become increasingly blurred. This means that the electrochemical corrosion process occurs more easily in the environment of unmodified artificial saliva.

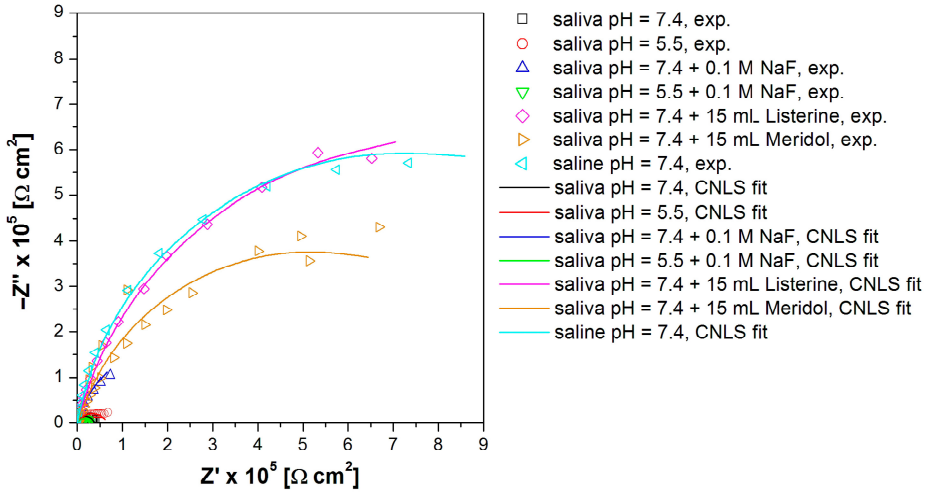

Figure 5. Experimental (symbols) and simulated (lines) Nyquist diagrams in the form Z''= f(Z') for the CoCrMo electrode in the applied corrosion environments at a temperature of 37 °C.

The Bode diagrams presented in Figures 6 and 7 confirm a very good fit of the experimental data to the software-generated model curve. The value of the phase angle shift provides important information about the mechanism and kinetics of the ongoing corrosion processes. Obtaining the shape of Bode diagrams in the form Φ = f(logf) visible in Figure 6 is characteristic of pitting corrosion occurring on the passivated material [5,8,13,30]. The increase in the value of the phase angle shift is proportional to the increase in the corrosion resistance of the material. Moreover, in Figure 6 there is only one time constant for the samples tested in all environments, which means that the electrochemical corrosion process took place in one stage. The Φ = f (logf) graphs are characterized by a wide plateau range visible for the middle frequencies and one maximum, which proves the high corrosion resistance of the passivated material. The tested alloy owes such high resistance to the elements Cr and Mo, which are characterized by excellent resistance in extremely aggressive corrosive environments. The widest plateau ranges are observed for the CoCrMo electrode in an

Preprints (www.preprints.org) | NOT PEER-REVIEWED | Posted: 19 October 2023 doi:10.20944/preprints202310.1223.v1

artificial saliva environment with the addition of Meridol® and Listerine® mouthwashes. The narrowest plateau range is characterized by the tested electrode in a solution of artificial saliva with pH = 7.4. The remaining environments have very similar plateau ranges.

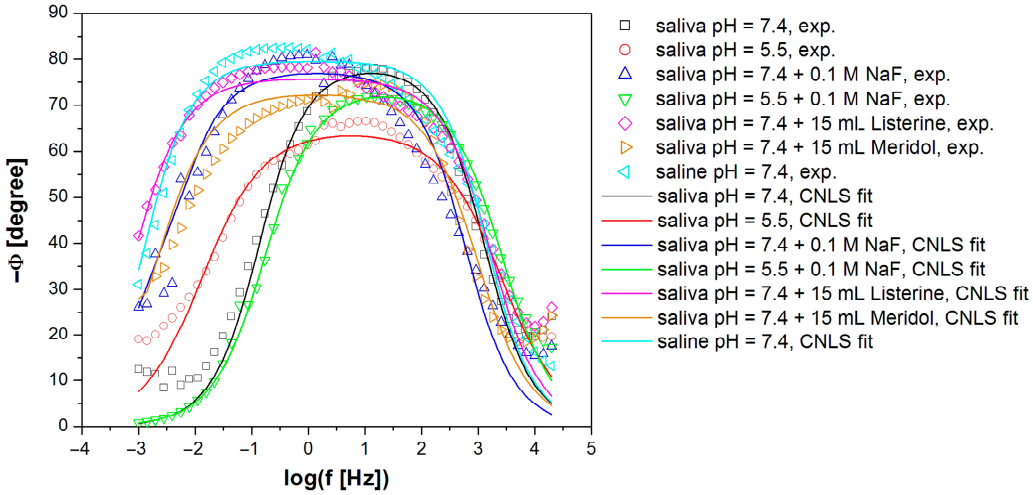

Figure 6. Experimental (symbols) and simulated (lines) Bode diagrams in the form and Φ=f(log f) for the CoCrMo electrode in the applied corrosion environments at a temperature of 37 °C.

The Bode plot in the form log|Z|=f(log f) provides information about the corrosion resistance of the tested material in a given environment (Figure 7). The highest corrosion resistance is demonstrated by the sample in the environment of artificial saliva at neutral pH with the addition of NaF, the value of the logarithm of the impedance modulus at the lowest tested frequency f = 1 mHz is 6.06 Ω cm². A slight decrease in the value of log $|Z|_{f=1\ mHz}$ = 6.03 Ω cm² was observed in the case of the sample tested in the saline environment. For an artificial saliva with pH = 7.4 with the addition of Meridol® mouthwash (log $|Z|_{f=1\ mHz}$ = 5.9 Ω cm²) and Listerine® (log $|Z|_{f=1\ mHz}$ = 5.94 Ω cm²) we observe a slight difference in the impedance modulus, which is caused by the different chemical composition of the added fluids. One of the basic factors influencing the corrosion resistance of a material is the chemical composition of the corrosive environment. In an acidic artificial saliva solution after modifying the environment with NaF, the value of log $|Z|_{f=1\ mHz}$ is 5.32 Ω cm² and in a neutral environment with the addition of NaF, log $|Z|_{f=1\ mHz}$ is 6.06 Ω cm². In the environment of neutral artificial saliva, the value of log $|Z|_{f=1\ mHz}$ is 4.62 Ω cm² and this is the lowest value obtained in impedance tests, which is associated with the lowest corrosion resistance of the sample in this environment. Figure 7 clearly shows that the corrosion resistance of the CoCrMo electrode is in the range between good and basic protection against electrochemical corrosion. Depending on the modifiers added to the tested environment, we can increase the corrosion resistance of the tested material.

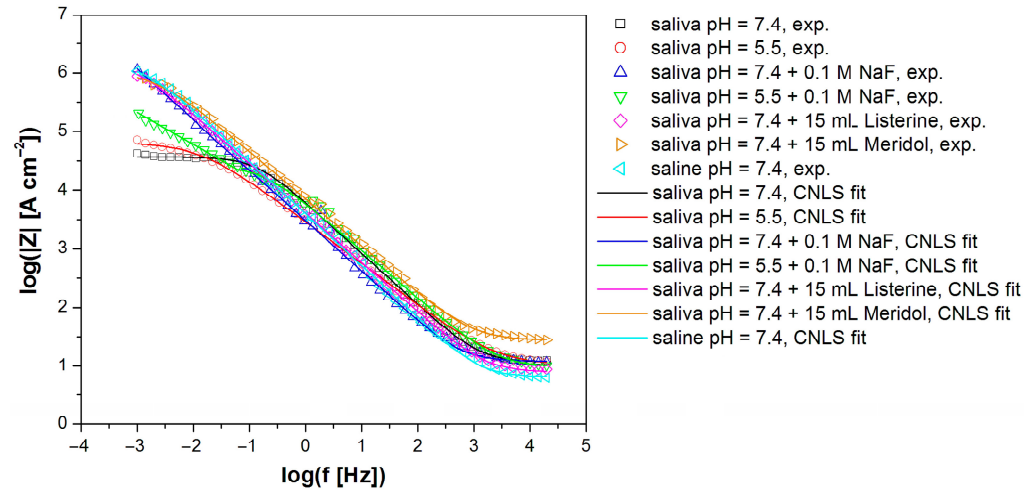

Preprints (www.preprints.org) | NOT PEER-REVIEWED | Posted: 19 October 2023 doi:10.20944/preprints202310.1223.v1

Figure 7. Experimental (symbols) and simulated (lines) Bode diagrams in the form log|Z|=f(log f) for the CoCrMo electrode in the applied corrosion environments at a temperature of 37 °C.

In the case of a NaF-modified artificial saliva solution, fluoride ions act to improve the corrosion resistance of the CoCrMo electrode. The drop in pH (acidification) accelerates corrosion due to the increased intensity of hydrogen depolarization. The corrosion rate increases significantly in the presence of aggressive chloride ions (Cl). Additionally, chloride ions inhibit the formation of passive layers and can also penetrate the oxide layer through pores or lattice defects and destroy it, which then leads to corrosion of deeper parts of the metal. In order to explain the impedance behavior of the CoCrMo electrode in the tested corrosion environments, the model of the electrical equivalent circuit CPE1, presented in Figure 4, was used. The detailed error in determining the parameters was below 28% (Table 3). The ϕ values ranged from 0.720 to 0.881.

Table 3. Parameters of the electrical equivalent circuit obtained on the basis of CNLS fitting of experimental EIS data for the CoCrMo electrode in the biological environment at 37 °C (see Figures 5–7).

Electrolyte Type	R_1 (Ω cm^2)	CPE_1-T (F cm^{-2} s$^{\phi\ 1}$)	CPE_1-ϕ	R_2 (Ω cm^2)	C_{dl} (F cm^{-2})
Saliva pH = 7.4 [30]	11.72(92)	0.74(9) × 10^{-5}	0.880(14)	3.71(21) × 10^4	4.11 × 10^{-6}
Saliva pH = 5.5	10.33(65)	0.24(2) × 10^{-5}	0.720(6)	6.6(11) × 10^4	7.72 × 10^{-6}
Saliva pH = 7.4 + 0.1 M NaF	12.13(63)	0.14(12) × 10^{-4}	0.862(8)	4.10(35) × 10^5	7.00 × 10^{-6}
Saliva pH = 5.5 + 0.1 M NaF	9.64(61)	0.37(3) × 10^{-5}	0.820(10)	2.71(16) × 10^4	7.77 × 10^{-7}
Saliva pH = 7.4 + 15 mL Listerine®	7.79(32)	0.83(4) × 10^{-5}	0.843(4)	1.59(16) × 10^6	5.26 × 10^{-6}
Saliva pH = 7.4 + 15 mL Meridol®	27.43(35)	0.27(6) × 10^{-5}	0.800(16)	1.03(29) × 10^6	9.97 × 10^{-7}
Saline pH = 7.4	6.39(34)	0.14(9) × 10^{-4}	0.881(5)	1.43(17) × 10^6	7.81 × 10^{-6}

The R_{ct} parameter is characterized by the highest value of 1.59(16) × 10^6 Ω cm^2 for the electrode in the environment of artificial saliva with the addition of Listerine® mouthwash, which has the strongest protective properties (Table 3). The corrosion resistance decreases successively, but it is of the same order of 10^6 in saline, and saliva with pH = 7.4 with the addition of Meridol® mouthwash. The electrode in artificial saliva solution with pH = 7.4 + 0.1 M NaF decreases by an order of magnitude. Saliva with pH = 5.5 before (R_{ct} = 6.6(11) × 10^4 Ω cm^2) and after addition of NaF (R_{ct} = 2.71(16) × 10^4 Ω cm^2), and in saliva with pH = 7.4 (R_{ct} = 3.71(21) × 10^4 Ω cm^2) are characterized by the lowest R_{ct} values. The smaller the R_2, the faster kinetics of the pitting corrosion of the CoCrMo electrode.

Determining by extrapolation a straight line with a slope equal to –1 in the Bode system log |Z| = f(logf) allows you to determine the parameter determining the capacity of the electrical double layer (C_{dl}) (Table 3). The high C_{dl} value indicates a greater exposure of the CoCrMo electrode surface to pitting corrosion due to the faster kinetics of the electrochemical process. Based on the discussion of the results obtained using the EIS method, it can be concluded that the corrosion resistance of the CoCrMo dental alloy has improved, caused by the presence of Meridol® and Listerine® mouthwashes in a neutral environment. Both the acidic reaction of the environment and the presence of Cl ions reduced the corrosion resistance of the tested electrode in the environment of body fluids. Chloride anions initiate the growth and expansion of pits on the self-passive oxide layer on the electrode surface and were the main cause of the deterioration of parameters such as R_{ct}, which is confirmed by the values of the corrosion current density determined in direct current electrochemical tests. The C_{dl} values for the CoCrMo electrode in a physiological saline are relatively high, which proves the material's high ability to corrode in an environment containing Cl ions.

The addition of NaF to the artificial saliva environment reduced the C_{dl} value in both acidic and neutral environments. The increase in R_{ct} value is caused by modifiers of the corrosive environment in the form of mouthwashes. A change in the pH of the electrolyte may destabilize the passive layer due to local anodic reactions. The drop in pH means that there is an increased concentration of H^+ ions due to the hydrolysis of cations, which makes it harder for the passive film to form and for

Preprints (www.preprints.org) | NOT PEER-REVIEWED | Posted: 19 October 2023 doi:10.20944/preprints202310.1223.v1

corrosion reactions to occur more easily. The additives used, although in small amounts, have a significant impact on individual corrosion resistance parameters. The use of EIS allowed for the determination of parameters defining the mechanism of the corrosion processes occurring. It was found that this is an activation mechanism, which involves transferring charged particles to the outside, resulting from the dissolution of the material, through the corrosive environment, where they combine with ions coming from the corrosive environment. The result of such a connection is the formation of a passive layer - a protective layer of the material.

3.5. In Vitro Electrochemical Tests Using the Potentiodynamic Method

The next stage of electrochemical research was the use of the potentiodynamic method to determine the susceptibility of the CoCrMo electrode to pitting corrosion in the tested environments. The obtained anodic polarization curves, showing the relationship log| |j = f(E) for the tested material in body fluid solutions, are presented in Figure 8. These tests were carried out at a polarization rate v = 1 mV s $^{-1}$. The current density values were logarithmized in order to determine the parameters characterizing the corrosion resistance of the tested electrode in particular environments. The CoCrMo electrode showed passive behavior in each tested environment, thanks to its optimal chemical composition, where the Cr and Mo content was within the limits ensuring the highest corrosion resistance [29].

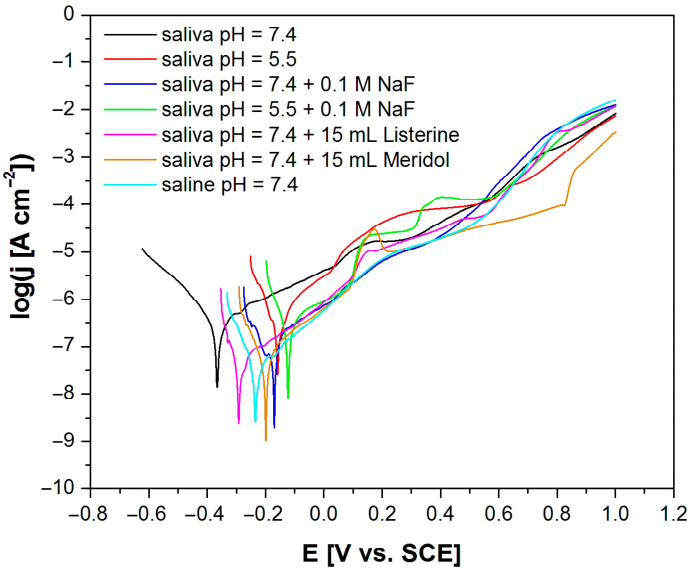

Figure 8. Anodic polarization curves for the CoCrMo electrode in the applied corrosion environments at 37 °C.

The values of the corrosion potential determined for the tested material in individual environments vary depending on the pH of the solutions used and the presence of additives in the form of mouthwashes and NaF introduced into the solutions as modifiers. The corrosion potential of the tested electrode varies depending on the environment used. The most negative (cathodic) value was shown by the CoCrMo in artificial saliva solution with pH = 7.4 (E_{cor} = 365 mV) [30]. A strongly cathodic value of the corrosion potential was also observed in a saline (E_{cor} = 237 mV). The CoCrMo alloy tested in the environment of artificial saliva with the addition of Listerine® and Meridol® mouthwasesh has similar values of corrosion potential, E_{cor} = 295 and 203 mV, respectively. In the artificial saliva solution with pH = 7.4 and pH = 5.5 enriched with NaF, we observe the most positive value of the corrosion potential, E_{cor} = 174 and 128 mV, respectively. This is related to the presence of fluoride anions in the solution, which facilitate the formation of a chromium(III) oxide layer on the electrode surface, in accordance with Okamoto's theory [32]. Corrosion damage in is caused by the adsorption of aggressive chloride ions on the metal surface, which penetrate through the passive

 doi:10.20944/preprints202310.1223.v1

layer. Chloride anions hinder the incorporation of metal ions into the metal layer and facilitate their penetration into the solution.

Based on the obtained electrochemical results, a three-layer model of the formation of a passive layer on the CoCrMo alloy in the tested corrosion environments can be proposed. It describes the process and chemical description of the reaction of creating a passive layer on the tested material. When the CoCrMo alloy (electrode) is immersed in the corrosive medium used and external voltage is applied to the system, the solution | electrode, chromium dissolution is initiated according to the Pourbaix diagram [33]. The ongoing process of active chromium dissolution is described by the reaction:

$$Cr \rightarrow (Cr)^{n+} + ne^{-}. \quad (2)$$

Chromium cations enter the solution to reach a lower energy level. On the surface of the material, they combine with oxygen ions to form the nuclei of a passive layer. The continuous increase in potential causes the growth of chromium oxide on the surface of the material and a passive layer is eventually formed according to the formula:

$$2\,CrO_4^{2-} + 6\,H^+ + 6e^- \rightarrow Cr_2O_3 + 4OH^- + H_2O. \quad (3)$$

The reaction in a medium with the addition of Cl ions proceeds as follows:

$$(Cr)^{n+}\,Cl^-_n + mH_2O \rightarrow Cr(OH)_n + 2mH^+ + nHCl. \quad (4)$$

After dissolution of the "protective" layer, the active state returns, which is associated with another intense impact of the environment on the material, and there is effective evolution of oxygen on the surface of the layer and from the dissolved passive layer itself (which has been observed experimentally) according to the formula:

$$O_2 + 4H^+ + 4e^- \rightarrow 2H_2O. \quad (5)$$

and the beginning of the processes of pitting on the surface of the material. The thickness of the entire protective layer ranges from several to several nanometers.

The metallic cobalt dissolution reaction, in accordance with the thermodynamic data for the Co-H_2O system, presented in the form of a Pourbaix diagram [32], proceeds as follows:

$$Co^0 + 2H^+ \rightarrow Co^{2+} + H_2. \quad (6)$$

Chromium dissolution reaction []:

$$Cr^{3+} + H_2O \leftrightarrow Cr(OH)^{2+} + H^+, \quad (7)$$

$$Cr(OH)^{2+} + H_2O \leftrightarrow Cr(OH)^{2-} + H^+, \quad (8)$$

$$Cr(OH)_3(S) \leftrightarrow Cr^{3+} + 3OH^-. \quad (9)$$

The molybdenum dissolution reaction occurs according to the reaction:

$$Mo^{3+} + 2H_2O \leftrightarrow MoO_2 + 4H^+ + e. \quad (10)$$

3.6. Scanning Kelvin Probe Study of the CoCrMo Alloy Surface

Using the SKP method, the surfaces of CoCrMo electrode subjected to the corrosion process in various solutions were analyzed. The SKP technique allowed for the determination of the contact potential difference (CPD) distribution on the sample surface (Figure 9).

Preprints (www.preprints.org) | NOT PEER-REVIEWED | Posted: 19 October 2023 doi:10.20944/preprints202310.1223.v1

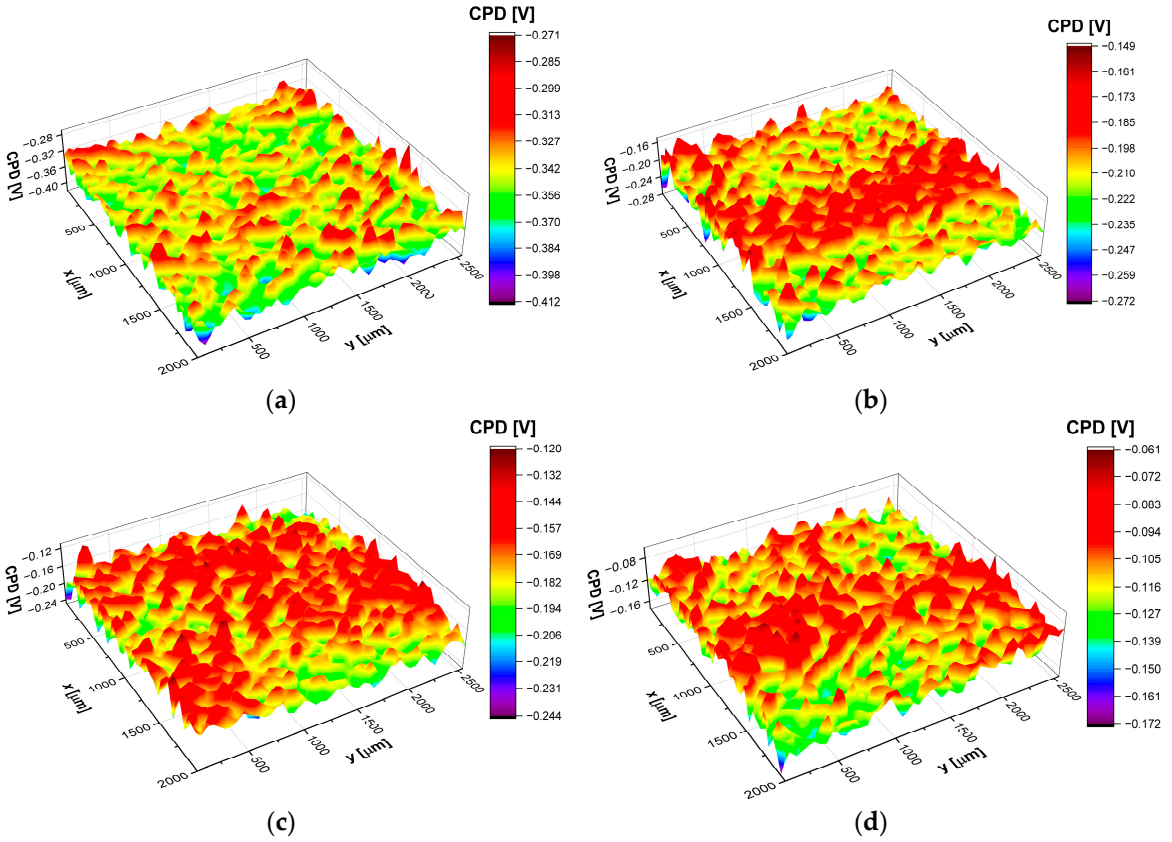

Figure 9. Exemplary contact potential difference (CPD) map for the CoCrMo electrode after corrosion tests in: (**a**) Saliva pH = 7.4; (**b**) Saliva pH = 7.4 + 15 mL Meridol®; (**c**)) Saliva pH = 7.4 + 0.1 M NaF; (**d**) Saliva pH = 5.5.

Based on the registered 3D maps, parameters characterizing the surface state, such as the arithmetic average of CPD heights (CPD_{av}), the root mean square deviation of CPD heights (CPD_{rms}), the skewness (CPD_{sk}), and the kurtosis (CPD_{ku}), were determined and are shown in Table 4. It was found that the highest average value of contact potential difference is obtained for sample tested in saliva pH = 5.5. Samples after corrosion tests in saliva pH = 5.5 + 0.1 M NaF and saliva pH = 7.4 + 0.1 M NaF exhibited approximately 50% lower values of CPD_{av} compared to sample after test in saliva pH = 5.5. In turn, the CPD_{av} determined for sample after test in saliva pH = 7.4 + 15 mL Meridol® was lower by around 80%. For samples tested in saline pH = 7.4, saliva pH = 7.4 + 15 mL Listerine®, and saliva pH = 7.4, the averages of measured CPD heights were 2.1, 2.7, and 3.1 times lower, respectively, compared to sample after test in saliva pH = 5.5. The CPD_{av} parameter suggests that sample tested in saliva pH = 5.5 exhibits the lowest electrochemical activity among all the tested samples. In contrast sample after corrosion tests in saliva pH = 7.4, has the most electrochemically active surface. Keeping in mind that the material from which the samples were made was the same and that the samples underwent similar potential-current treatments, it can be concluded that measured values of CPD_{av} depend on the composition of the solution. Thus, sample tested in saliva pH = 5.5 is most likely subjected to the least aggressive environment, whereas sample studied in saliva pH = 7.4 was soaked in the most aggressive one.

Preprints (www.preprints.org) | NOT PEER-REVIEWED | Posted: 19 October 2023 doi:10.20944/preprints202310.1223.v1

Table 4. Statistical parameters calculated using CPD maps of the CoCrMo alloy; CPD_{av} is the arithmetic average, CPD_{rms} is the root mean square deviation, CPD_{sk} is the skewness, and CPD_{ku} is the excess kurtosis.

Electrolyte type	CPD_{av} [mV]	CPD_{rms} [mV]	CPD_{sk}	CPD_{ku}
saliva pH = 7.4	−346.3	18.6	0.001	0.10
saliva pH = 5.5	−112.6	16.5	0.05	−0.14
saliva pH = 7.4 + 0.1 M NaF	−172.7	17.7	−0.06	0.04
saliva pH = 5.5 + 0.1 M NaF	−169.3	16.4	−0.12	0.06
saliva pH = 7.4 + 15 mL Listerine®	−306.0	21.0	0.17	0.13
saliva pH = 7.4 + 15 mL Meridol®	−204.6	17.5	−0.07	0.21
saline pH = 7.4	−235.6	16.6	−0.08	0.11

The CPD_{rms} values determined for samples in all corrosion solutions vary from 17 mV to 21 mV. This indicates that the deviation of CPD heights from the the average value is comparable for all the investigated samples. Skewness and kurtosis quantitatively describe the shape of the CPD distribution. As shown in Table 4, both parameters vary from about −0.1 to about 0.2, indicating that the CPD distribution is of a Gaussian type. Moreover, CPD_{sk} and CPD_{ku} close to zero indicate that the contact potential difference heights are symmetrically distributed around the average and that no areas with relatively large/small CPD values are observed on the examined surfaces.

5. Conclusions

The results of the research obtained in this study were the basis for formulating the following conclusions:

Tests of corrosion resistance of Bego Wirobond® C dental alloy CoCrMo alloy containing Co 59.8(8) wt.%, Cr 31.5(4) wt.%, and Mo 8.8(6) wt.% in the environment of artificial saliva before and after modification with NaF and Listerine® and Meridol® mouthwashes, and comparatively in a physiological saline solution revealed the susceptibility of the tested material to pitting corrosion. The results obtained using the anodic polarization curves j=f(E) confirmed the passivation process taking place on the tested material. The lowest corrosion resistance was obtained in the artificial saliva solution with pH = 7.4. The highest corrosion resistance for the CoCrMo dental alloy after electrochemical tests was obtained in a saliva solution with pH = 5.5 with the addition of NaF. The corrosion resistance of the CoCrMo alloy is related to the chemical composition of the environment in which the corrosion tests were carried out. The results obtained were unambiguous indicate the influence of modification of the artificial saliva environment on the resistance of the CoCrMo dental alloy.It was shown that F ions contributed to the improvement of corrosion resistance in the artificial saliva environment by supporting the construction of the passive layer.

The use of electrochemical impedance spectroscopy in the study of pitting corrosion occurring on the CoCrMo alloy in the tested corrosion environments allowed for the characterization of the impedance of the electrode | solution interface for by approximating the impedance data using the CPE1 model of the electrical equivalent circuit. On the basis of the obtained impedance spectra, the activation mechanism of corrosion processes was found in all subjects environments.

The SKP characterization of the CoCrMo alloy after corrosion tests revealed the effect of artificial saliva modification on electronic properties of Bego Wirobond® C dental alloy.

Author Contributions: Conceptualization, B.Ł. and K.G.; methodology, B.Ł., P.O. and J.K.; validation, P.O., J.K. and K.G.; formal analysis, B.Ł., P.O., J.K. and K.G.; investigation, B.Ł., P.O., J.K. and K.G.; resources, B.Ł. and K.G.; data curation, P.O. and J.K.; writing—original draft preparation, B.Ł., P.O. and J.K.; writing—review and editing, K.G.; visualization, P.O. and J.K.; funding acquisition, B.Ł. All authors have read and agreed to the published version of the manuscript.

Funding: This research received no external funding.

Institutional Review Board Statement: Not applicable.

Informed Consent Statement: Not applicable.

Data Availability Statement: MDPI Research Data Policies.

Conflicts of Interest: The authors declare no conflict of interest.

References

1. Petković Didović, M.; Jelovica Badovinac, I.; Fiket, Ž.; Žigon, J.; Rinčić Mlinarić, M.; Čanadi Jurešić, G. Cytotoxicity of Metal Ions Released from NiTi and Stainless Steel Orthodontic Appliances, Part 1: Surface Morphology and Ion Release Variations. *Materials* **2023**, *16*, 4156. https://doi.org/10.3390/ma16114156.
2. Robles, D.; Brizuela, A.; Fernández-Domínguez, M.; Gil, J. Corrosion Resistance and Titanium Ion Release of Hybrid Dental Implants. *Materials* **2023**, *16*, 3650. https://doi.org/10.3390/ma16103650.
3. Correa-Rossi, M.; Romero-Resendiz, L.; Leal-Bayerlein, D.; Garcia-Alves, A.L.; Segovia-López, F.; Amigó-Borrás, V. Mechanical, Corrosion, and Ion Release Studies of Ti-34Nb-6Sn Alloy with Comparable to the Bone Elastic Modulus by Powder Metallurgy Method. *Powders* **2022**, *1*, 3-17. https://doi.org/10.3390/powders1010002.
4. Arakelyan, M.; Spagnuolo, G.; Iaculli, F.; Dikopova, N.; Antoshin, A.; Timashev, P.; Turkina, A. Minimization of adverse effects associated with dental alloys. *Materials* **2022**, *15*, 7476. https://doi.org/10.3390/ma15217476.
5. Dudek, K.; Dulski, M.; Łosiewicz, B. Functionalization of the NiTi shape memory alloy surface by HAp/SiO_2/Ag hybrid coatings formed on SiO_2-TiO_2 glass interlayer. *Materials* **2020**, *13*, 1648. https://doi.org/10.3390/ma13071648.
6. Aniołek, K.; Łosiewicz, B.; Kubisztal, J.; Osak, P.; Stróż, A.; Barylski, A.; Kaptacz, S. Mechanical properties, corrosion resistance and bioactivity of oxide layers formed by isothermal oxidation of Ti–6Al–7Nb alloy. *Coatings* **2021**, *11*, 505. https://doi.org/10.3390/coatings11050505.
7. Zatkalíková, V.; Halanda, J.; Vaňa, D.; Uhríčik, M.; Markovičová, L.; Štrbák, M.; Kuchariková, L. Corrosion Resistance of AISI 316L Stainless Steel Biomaterial after Plasma Immersion Ion Implantation of Nitrogen. *Materials* **2021**, *14*, 6790. https://doi.org/10.3390/ma14226790.
8. Szklarska, M.; Dercz, G.; Simka, W.; Łosiewicz, B. A.c. impedance study on the interfacial properties of passivated Ti13Zr13Nb alloy in physiological saline solution. *Surf. Interface Anal.* **2014**, *46*, 698–701. https://doi.org/10.1002/sia.5383.
9. Motoyoshi, M. (Ed.). *Current Techniques and Materials in Dentistry*, Publisher: MDPI AG, 2022, ISBN: 3036544135.
10. Givan, D.A. Precious metal alloys for dental applications. *Precious Metals for Biomedical Applications* **2014**,109–129. https://doi.org/10.1533/9780857099051.2.109.
11. Sinyakova, E.F.; Vasilyeva, I.G.; Oreshonkov, A.S.; Goryainov, S.V.; Karmanov, N.S. Formation of Noble Metal Phases (Pt, Pd, Rh, Ru, Ir, Au, Ag) in the Process of Fractional Crystallization of the $CuFeS_2$ Melt. *Minerals* **2022**, *12*, 1136. https://doi.org/10.3390/min12091136.
12. Stróż, A.; Dercz, G.; Chmiela, B.; Stróż, D.; Łosiewicz, B. Electrochemical formation of second generation TiO_2 nanotubes on Ti13Nb13Zr alloy for biomedical applications. *Acta Phys. Pol.* **2016**, *130*, 1079–1080. https://doi.org/10.12693/APhysPolA.130.1079.
13. Łosiewicz, B.; Osak, P.; Maszybrocka, J.; Kubisztal, J.; Stach, S. Effect of autoclaving time on corrosion resistance of sandblasted Ti G4 in artificial saliva. *Materials* **2020**, *13*, 4154. https://doi.org/10.3390/ma13184154.
14. Padrós, R.; Giner-Tarrida, L.; Herrero-Climent, M.; Punset, M.; Gil, F.J. Corrosion Resistance and Ion Release of Dental Prosthesis of CoCr Obtained by CAD-CAM Milling, Casting and Laser Sintering. *Metals* **2020**, *10*, 827. https://doi.org/10.3390/met10060827.
15. Uriciuc, W.A.; Boșca, A.B.; Băbțan, A.-M.; Vermeșan, H.; Cristea, C.; Tertiș, M.; Păscuță, P.; Borodi, G.; Suciu, M.; Barbu-Tudoran, L.; Popa, C.O.; Ilea, A. Study on the Surface of Cobalt-Chromium Dental Alloys and Their Behavior in Oral Cavity as Cast Materials. *Materials* **2022**, *15*, 3052. https://doi.org/10.3390/ma15093052.
16. Kajzer, W.; Szewczenko, J.; Kajzer, A.; Basiaga, M.; Jaworska, J.; Jelonek, K.; Nowińska, K.; Kaczmarek, M.; Orłowska, A. Physical Properties of Electropolished CoCrMo Alloy Coated with Biodegradable Polymeric Coatings Releasing Heparin after Prolonged Exposure to Artificial Urine. *Materials* **2021**, *14*, 2551. https://doi.org/10.3390/ma14102551.
17. A. Mace; P. Khullar; C. Bouknight; J.L. Gilbert. Corrosion properties of low carbon CoCrMo and additively manufactured CoCr alloys for dental applications. Dental Materials 2022, 38(7), 1184-1193. https://doi.org/10.1016/j.dental.2022.06.021.
18. *ISO 10271:2021*; Dentistry — Corrosion test methods for metallic materials. ISO: Geneva, Switzerland, 2021.

19. *ISO 22674:2023-03;* Dentistry — Metallic materials for fixed and removable restorations and appliances. ISO: Geneva, Switzerland, 2023.
20. *ISO 9693-1:2012;* Dentistry — Compatibility testing - Part 1: Metal-ceramic systems. ISO: Geneva, Switzerland, 2012.
21. *ISO 13485:2016-04;* Medical devices — Quality management systems — Requirements for regulatory purposes. ISO: Geneva, Switzerland, 2012.
22. https://www.tehnicaldent.ro/11606-wirobond-c (accessed on 10.10.2023).
23. https://gyenesdent.at/zahnersatz-gyor-ungarn (accessed on 10.10.2023).
24. https://bnb-dental.com/producto/wirobond-c-bego-por-1gr (accessed on 11.10.2023).
25. *ISO 10993-5:2009*; Biological evaluation of medical devices — Part 5: Tests for in vitro cytotoxicity. ISO: Geneva, Switzerland, 2009.
26. *ISO 6507-1:2018-05;* Metallic materials — Vickers hardness test — Part 1: Test method. ISO: Geneva, Switzerland, 2018.
27. *AFNOR/NF standard S90-701*; Matériel médico-chirurgical — Biocompatibilité des matériaux et dispositifs médicaux — Méthodes d'extraction. French Standardization Association: Paris, France, 1988.
28. Boukamp, B.A. A Linear Kronig-Kramers transform test for immittance data validation. *J. Electrochem. Soc.*, **1995**, *142*(6), 1885–1894. https://doi.org/10.1149/1.2044210.
29. Branzoi, I.V.; Iordoc, M.; Codescu, M.M. Corrosion behaviour of CoCrMo and CoCrTi alloys in simulated body fluids. *UPB Scientific Bulletin, Series B: Chemistry and Materials Science* **2007**, 69(4):11-18.
30. Łosiewicz, B.; Osak, P.; Górka-Kulikowska, K. Electrophoretic Deposition of Multi-Walled Carbon Nanotubes Coatings on CoCrMo Alloy for Biomedical Applications. *Micromachines* (under review).
31. Lasia, A. *Electrochemical Impedance Spectroscopy and Its Applications*; Springer Science + Business Media: New York, NY, USA, 2014; ISBN 978-1-4614-8932-0.
32. Okamoto, G. Passive film of 18-8 stainless steel structure and its function. *Corrosion Science*, **1973**, *13*(6), 471–489. https://doi.org/10.1016/0010-938x(73)90031-0.
33. *Atlas of Eh-pH diagrams*. Intercomparison of thermodynamic databases. Geological Survey of Japan Open File Report No.419.